Identification of TFR2 as a novel ferroptosis-related gene that serves an important role in prognosis and progression of triple-negative breast cancer

YAN YANG[1-3], JIE DU[2], YUN-FEI HUANG[2], WEI HE[2], LI LIU[4], DAN LI[4] and RUI CHEN[5]

[1]Department of Laboratory Medicine, Affiliated Hospital of Zunyi Medical University; Schools of [2]Laboratory Medicine and [3]Forensic Medicine; [4]Clinical Medical College, Zunyi Medical University; [5]Department of General Surgery, Affiliated Hospital of Zunyi Medical University, Zunyi, Guizhou 563003, P.R. China

Received August 28, 2023; Accepted November 16, 2023

DOI: 10.3892/ol.2023.14176

Abstract. Effective targeted therapeutic strategies for triple-negative breast cancer (TNBC), the most malignant subtype of breast cancer, are currently lacking. Ferroptosis has been reported to be associated with the onset and advancement of various cancer types, including TNBC. However, there are limited studies on the correlation between TNBC and ferroptosis-related genes. In addition, the potential biomarkers of ferroptosis in TNBC need further investigation. The present study aimed to assess the prognostic role of a novel ferroptosis-related gene signature in the context of TNBC. The signature was established utilizing The Cancer Genome Atlas dataset. This three-gene model [transferrin receptor 2 (TFR2), regulator of G protein signaling 4 and zinc finger protein 36] was developed utilizing least absolute shrinkage and selection operator regression analysis and demonstrated satisfactory predictive performance in TNBC. The area under the curve values of the receiver operating characteristic curves in this model concerning the 1-, 2- and 3-year survival prediction were 0.721, 0.840 and 0.856, respectively. The predictive performance of the model was verified using the TNBC dataset GSE25307. Gene set enrichment analysis (GSEA) demonstrated the enrichment of genes in the low-risk group in a number of important metabolic pathways. Single-sample GSEA demonstrated a variation in the expression levels of immune checkpoint molecules between the high- and low-risk groups. The inhibitory impact of TFR2 knockdown on the proliferative capacity of TNBC cells was verified through *in vitro* experiments. The data also demonstrated that TFR2 knockdown facilitated the ferroptosis of TNBC cells. Additional assessments indicated that the effects of TFR2 knockdown were partially reversed upon treatment with the ferroptosis inhibitor ferrostatin-1. In conclusion, in the present study, a novel and accurate ferroptosis-related predictive signature was established for TNBC with potential future clinical applications. To the best of our knowledge, the present study is the first to report that TFR2 regulated ferroptosis in TNBC cells *in vitro*.

Correspondence to: Dr Rui Chen, Department of General Surgery, Affiliated Hospital of Zunyi Medical University, 149 Dalian Road, Zunyi, Guizhou 563003, P.R. China
E-mail: chenrui1983105@163.com

Key words: triple-negative breast cancer, ferroptosis, gene signature, prognosis, transferrin receptor 2

Introduction

Breast cancer, a heterogenous type of tumor with the highest incidence rate among women worldwide, accounting for 31.0% of all female cancer cases, is accountable for a high incidence of cancer-associated mortalities (1). Based on the genome sequence and protein expression levels of human epidermal growth factor 2 (HER2), progesterone receptor (PR) and estrogen receptor (ER), breast cancer can be divided into luminal, HER2-enriched and triple-negative types (2). Triple-negative breast cancer (TNBC), the most malignant subtype, is linked to a highly unfavorable prognosis and poor overall survival (OS) rates compared with other subtypes (3). In addition, the current therapeutic strategies for TNBC are limited due to a lack of clear targets and chemotherapy remains the main treatment modality for TNBC. Although certain aggressive TNBC types are immunogenic, the majority of patients exhibit limited responses to immunotherapy (4,5). Therefore, it is essential to explore new targets for developing novel therapies for TNBC.

Ferroptosis, a unique iron-dependent cell death process, is distinct from apoptosis, necrosis and autophagy. A key hallmark of ferroptosis is enhanced generation of intracellular reactive oxygen species (ROS) and diminished mitochondrial volume (6). It has previously been reported that iron metabolism-mediated ROS accumulation promotes ferroptosis. Furthermore, ferroptosis-related genes, which regulate ferroptosis, participate in the onset and progression of a number of malignancies, including breast cancer (7,8). For instance, glutathione peroxidase 4 (GPX4), a core regulatory gene involved in ferroptosis, is negatively associated with the prognosis of breast cancer, as its expression enhances ferroptosis in

cells (9). Analyzing the expression levels of acyl-CoA synthetase long chain family member 4, which promotes ferroptosis by upregulating intracellular lipids, can predict the response to neoadjuvant chemotherapy (10). Furthermore, a previous study reported that the induction of ferroptosis may overcome drug resistance and is a potential novel therapeutic approach for cancer (11). Of note, TNBC cells have been reported to be susceptible to ferroptosis due to their complex metabolic characteristics and cellular signaling pathways (12). TNBC cells can express high levels of the xCT cystine/glutamate antiporter, which leads to a reduction in xCT-associated glutathione levels, thus reducing cell viability and sensitizing the cells to ferroptosis (13). In addition, it has been reported that MDA-MB-231 TNBC cells are highly cystine-dependent and susceptible to ferroptosis (14,15). However, limited studies have examined the association of ferroptosis-related genes with TNBC prognosis. In addition, a specific ferroptosis-related therapeutic target for TNBC has not been identified to date.

In the present study, genes linked to ferroptosis were investigated using mRNA expression data and relevant clinical profiles from The Cancer Genome Atlas (TCGA) database. The objective of the current study was to provide valuable insight into guiding clinical decisions for TNBC treatment. Next, the model was further validated in a Gene Expression Omnibus (GEO) cohort and functional enrichment analysis was performed to explore the possible mechanisms of these identified genes in different risk groups classified using the developed model. In addition, the immune-related responses in TNBC were evaluated. Finally, the role of transferrin receptor 2 (TFR2) in TNBC was verified using *in vitro* experiments. The present findings further demonstrated the functions of ferroptosis-related genes and provided novel targets for potential therapeutic intervention in TNBC.

Materials and methods

Data collection. The clinical information and transcriptome of individuals with breast cancer were obtained from the TCGA (http://cancergenome.nih.gov/) database (added before May 1, 2022). For transcriptome data, after entering the file download interface (http://portal.gdc.cancer.gov/), 'TCGA-BRCA' project was selected in the Cases parameter. In the Files parameter section, 'transcriptome profiling' was selected in the data category, 'gene expression quantification' in the data type and 'HTSeq-FPKM' in the workflow type. For clinical data, 'clinical' was selected in the data category and 'bcr-xml' in the workflow type. The TCGA dataset comprised data from 1,096 breast cancer and 112 healthy breast tissue samples. To distinguish the molecular subtypes of patients with breast cancer, data from The University of California, Santa Cruz Xena website (https://xenabrowser.net/datapages/) corresponding to TCGA-BRCA were retrieved. The inclusion criteria for TNBC were based on the following immunohistochemical results: i) ER, PR and HER2 were negative; and ii) fluorescence *in situ* hybridization was required to be negative when the HER2 level was 2+. After molecular typing screening and excluding cases with a follow-up time of <90 days, the training dataset comprised 118 individuals with TNBC. In addition, the validation dataset was accessed at GEO (https://www.ncbi.nlm.nih.gov/geo/). The RNA expression data with follow-up information of individuals with TNBC (dataset accession no. GSE25307) were accessed at GEO and comprised data from 120 tumor samples. In brief, the series matrix file containing the original data of probe results and clinical information was downloaded and the probes were converted into the corresponding gene symbol according to the annotation information by the platform (GPL5354 SWEGENE H_v2.1.1 55K). General baseline clinical features of the individuals included in the two databases were analyzed, which comprised information such as age, tumor staging and prognosis (Table I). Furthermore, the data of 259 genes linked to ferroptosis were sourced from the FerrDb website (http://www.zhounan/org/ferrdb/; Table SI). These genes have also been reported by a previous study (16).

Detection of ferroptosis-related differentially expressed genes (DEGs). Ferroptosis-related DEGs in TNBC and healthy breast tissue samples were detected in TCGA cohort using the 'limma' R package (version 3.46.0) based on the following criteria: i) False discovery rate (FDR) of 0.05; and ii) log fold-change (FC) >1. Heatmaps were plotted to visualize DEGs. To assess these genes further, the Search Tool for the Retrieval of Interacting Genes and proteins (STRING; https://string-db.org) database was employed for establishing the interaction network of these identified DEGs. Cytoscape (version 3.8.2; https://cytoscape.org) was utilized for the visualization of the specific molecular regulatory association of DEGs.

Functional enrichment analysis. Ferroptosis-related DEGs in TNBC vs. healthy breast tissues were subjected to Gene Ontology (GO) (cellular component, molecular function and biological process) and Kyoto Encyclopedia of Genes and Genomes (KEGG) enrichment analyses (log FC ≥1; FDR <0.05) using the 'clusterProfiler' R package (version 3.18.1).

Construction of the prognostic ferroptosis-related gene signature. Univariate Cox regression analysis of OS was performed to identify ferroptosis-related prognostic DEGs utilizing the R 'survival' package (version 3.5-5). The expression difference of ferroptosis-related DEGs with prognostic significance in breast cancer and healthy breast tissue were analyzed through the Human Protein Atlas (HPA) database, which is an online tool (www.proteatlas.org) that displays immunohistochemistry results of protein expression patterns in cancer tissues, healthy tissues and different cell types. The resulting data were visualized using forest plots. Furthermore, the survival of patients with TNBC was examined through Kaplan-Meier (KM) Plotter (http://kmplot.com/analysis/), which integrates information on patients with TNBC from E-MTAB-365, E-TABM-43 and a series of GEO datasets (17). Next, least absolute shrinkage and selection operator (LASSO) Cox regression analysis was conducted utilizing the function 'glmnet' of R (version 4.1-7) to construct a prognostic model. The coefficients of the normalized expression level of the three aforementioned prognostic genes were calculated (Table SII).

Model assessment. The gene expression level was utilized to compute the risk score and its formula was as follows: Sum (expression level of each gene x corresponding coefficient). The categorization of the individuals under study into the

Table I. Clinicopathological parameters of the patients with triple negative breast cancer in the present study.

Patient characteristic	TCGA-BRCA (n=230)	GSE25307 (n=120)
Type of sample		
Tumor	118	120
Normal	112	0
Age, years	55 (29-85)	
Tumor stage		
I	20	
II	76	
III	17	
IV	2	
Unknown	3	
T stage		
T1	28	
T2	74	
T3	12	
T4	3	
Unknown	1	
N stage		
N0	75	
N1	29	
N2	8	
N3	6	
M stage		
M0	109	
M1	2	
Unknown	7	
Survival status		
Deceased	18	57
Alive	100	63
Median overall survival, days	1,606	2,777

Values are expressed as n or median (range) unless otherwise specified.

high- and low-risk score groups was performed according to their median risk score. Principal component analysis (PCA) and t-distributed stochastic neighbor embedding (t-SNE) were performed utilizing the 'Rtsne' (version 0.16) and 'stats' (version 4.1.1) R packages to assess the distribution of various groups. Furthermore, the model was examined concerning its predictive accuracy by plotting the time-dependent receiver operating characteristic (ROC) curve using the 'survivalROC' R package (version 1.0.3.1).

Survival analyses. Survival analysis of the high- and low-risk groups was performed using the 'survminer' (version 0.4.8) and 'survival' (version 3.5-5) R packages. The link between risk scores and clinicopathological characteristics in individuals with TNBC was examined using univariate and multivariate Cox analyses. The clinical benefits of risk scores were determined through decision curve analysis (DCA). The R package 'regplot' (version 1.1) was utilized to develop a nomogram integrating TNBC clinicopathological features and risk scores for the prediction of the OS of individuals at diverse time-points.

Gene set enrichment analysis (GSEA). GSEA was performed to identify relevant DEGs between the high- and low-risk groups employing the R package 'edgeR' (version 3.34.0) according to the following criteria: i) FDR <0.05; and ii) log2 FC ≥1. In addition, KEGG analysis provided further insight into the potential mechanisms of the risk signature in TNBC. P<0.05 and FDR q<0.05 were considered to indicate a statistically significant difference.

Immune analyses. To assess the immune cell types in patients with TNBC in the high- and low-risk groups, the CIBERSORT, CIBERSORT-ABS, EPIC, XCELL and MCPCOUNTER algorithms were used. The role of the ferroptosis-related risk signature in the immunotherapy response prediction of individuals with TNBC was examined using the 'ggplot2' (version 3.4.2) and 'ggpubr' (version 0.5.0) R packages. Single-sample GSEA (ssGSEA) was performed to evaluate the association of risk score with potential immune checkpoints.

Cell culture and reagents. Healthy breast epithelial cells (MCF-10A), luminal A breast cancer cells (T-47D), HER2-enriched breast cancer cells (SK-BR-3) and TNBC cells (BT-549, MDA-MB-468, MDA-MB-436 and MDA-MB-231) were purchased from Procell Life Science & Technology Co., Ltd., and luminal A breast cancer cells (MCF-7) and luminal B breast cancer cells (BT-474) were purchased from The Cell Bank of the Type Culture Collection of The Chinese Academy of Sciences. MDA-MB-231 and MDA-MB-468 cells were cultured in Gibco's Leibovitz's L-15 medium with 10% FBS (Thermo Fisher Scientific, Inc.). BT-549 cells were cultured in Gibco's RPMI-1640 basic medium (Thermo Fisher Scientific, Inc.) containing 0.01 mg/ml insulin (Beijing Solarbio Science & Technology Co., Ltd.) and 10% FBS. T-47D cells were cultured in Gibco's DMEM (Thermo Fisher Scientific, Inc.) supplemented with 10% FBS. MCF-7, SK-BR-3, MDA-MB-436 and BT-474 cells were cultured in Gibco's RPMI-1640 medium containing 10% FBS. MCF-10A cells were cultured in Gibco's DMEM containing 5% horse serum, 0.5 μg/ml cortisol, 0.01 mg/ml insulin and 1% non-essential amino acids (Procell Life Science & Technology Co., Ltd.). MDA-MB-468 and MDA-MB-231 cells were incubated at 37˚C under 100% humidity and 100% O_2. The remaining cell lines were incubated at 37˚C with 100% humidity and 5% CO_2. The cells used in the present study were authenticated using short tandem repeat profiling and were determined to be free of mycoplasma contamination. The ferroptosis inhibitor ferrostatin-1 (Fer-1; MedChemExpress) was stored at -80˚C.

Transfection and RNA interference. Three different small interfering RNAs (siRNAs) against TFR2, siRNA negative control (NC; Table SIII) and the GP-transfect-Mate transfection reagent sourced from Shanghai GenePharma Co., Ltd. Culture plates (6-well) were utilized for culturing cells (5x10^7 cells/l)

in their logarithmic growth phase for 24 h to achieve 60% density. siRNA or siNC (5 μl) and transfection reagent GP-transfect-Mate (4 μl) were added into 300 μl OPTI-MEM (Gibco; Thermo Fisher Scientific, Inc.) and incubated at room temperature for 20 min before being added to MDA-MB-436 cells, and the plate was incubated 48 h or 72 h under 5% CO_2 at 37˚C. The knockdown efficiency at 48 h or 72 h post-transfection was examined using reverse transcription-quantitative PCR (RT-qPCR) and western blot analyses.

RNA extraction and RT-qPCR analysis. The TFR2 mRNA expression level in MCF-10A, T-47D, MCF-7, SK-BR-3, BT-474, BT-549, MDA-MB-468, MDA-MB-436 and MDA-MB-231 cells was assessed using RT-qPCR. Extraction of total RNA from cells was performed utilizing RNAiso Plus (cat. no. 9108Q; Takara Biotechnology Co., Ltd.). Total RNA was then reverse-transcribed into complementary DNA using PrimeScript™ RT Master Mix (Takara Biotechnology Co., Ltd.) according to the manufacturer's protocol. qPCR analysis was performed utilizing TB Green™ Premix EX Taq™ II (Takara Biotechnology Co., Ltd.) in a GENTIER 96 qPCR instrument (Tianlong). The PCR conditions were as follows: Initial denaturation at 95˚C for 30 sec; and 40 cycles of 95˚C for 5 sec and 60˚C for 34 sec. The melting curve was generated under the following conditions: 95˚C for 15 sec, followed by 95˚C for 5 sec and 60˚C for 34 sec. GAPDH was used as an internal reference for normalization. The mRNA expression levels were determined using the $2^{-\Delta\Delta Cq}$ method (18). Table SIII contains the sequences of the primers utilized.

Cell viability analysis. The density of cells in the logarithmic growth phase was adjusted to $3x10^7$ cells/l. Cells were seeded into a 96-well plate (100 μl/well, $3x10^3$ cells/well) and the plate was incubated overnight under 5% CO_2 at 37˚C. Cells were then transfected with siRNA or siNC and incubated for 24, 48 and 72 h under 5% CO_2 at 37˚C. The culture medium was replaced at each time-point and the cells were then incubated with 110 μl complete medium containing 10 μl Cell Counting Kit (CCK)-8 reagent (Beijing Solarbio Science & Technology Co., Ltd.) for 90 min at 37˚C. The optical density of the reaction mixture was measured at 450 nm using a microplate reader (Thermo Fisher Scientific, Inc.).

Lipid peroxidation assay. Cells were cultured in T25 culture flasks to a density of 80%. Cells were lysed with a western blotting and immunoprecipitation cell lysis solution (cat. no. P0013; Beyotime Institute of Biotechnology). Next, the lysate was centrifuged at 12,000 x g for 10 min at 4˚C. A BCA protein assay kit (Epizyme) was utilized for determining the protein concentration in the supernatant for subsequent calculation of the malondialdehyde (MDA) content. The MDA content of the samples was determined utilizing a lipid peroxidation MDA assay kit (Beyotime Institute of Biotechnology). In brief, 100 μl of sample was incubated with 200 μl MDA assay working solution for 15 min in a water bath at 100˚C. Subsequently, the sample was centrifuged for 10 min at room temperature at 1,000 x g. The absorbance of 200 μl of the supernatant at 532 nm was measured using a microplate reader.

Western blot analysis. Extraction of total protein was conducted using a whole-cell lysis assay kit (cat no. KGP2100; Nanjing KeyGen Biotech Co., Ltd.), followed by quantification with a BCA protein assay kit (Epizyme). The proteins (15 μg per lane) were subjected to separation by 10% SDS-PAGE and then transferred onto a polyvinylidene fluoride membrane. Membranes were blocked using 8% skimmed milk in TBS with 0.1% Tween 20 at room temperature for 2 h, followed by incubation with anti-TFR2 (cat. no. ET7108-21; HUABIO; 1:1,000 dilution), anti-lysyl oxidase (LOX; cat. no. 17958-1-AP; Proteintech, Inc.; 1:1,000 dilution), anti-solute carrier family 7 member 11 (SLC7A11; cat. no. 12691; Cell Signaling Technology, Inc.; 1:1,000 dilution), anti-GPX4 (cat. no. ER1803-15; HUABIO; 1:1,000 dilution) and anti-ferritin heavy chain 1 (FTH1; cat. no. 4393; Cell Signaling Technology, Inc.; 1:1,000 dilution) primary antibodies overnight at 4˚C. Next, membranes were incubated with horseradish peroxidase-conjugated goat anti-rabbit IgG (cat. no. HA1001; HUABIO; 1:5,000 dilution) or goat anti-mouse IgG (cat. no. HA1006; HUABIO; 1:5,000 dilution) secondary antibodies at room temperature for 2 h. Immunoreactive signals were developed employing an enhanced chemiluminescence solution (Dalian Meilun Biology Technology Co., Ltd.) and visualized using a gel imaging system (ChemiDoc MP; Bio-Rad Laboratories, Inc.). The grayscale values of the protein bands were derived utilizing Gel-Pro analyzer 4.0 (Media Cybernetics, Inc.) to calculate the relative expression levels of proteins. Anti-GAPDH antibodies (cat. no. EM1101; HUABIO; 1:5,000 dilution) were used to detect GAPDH, which functioned as an internal control for normalization.

Statistical analysis. A total of 118 patients with TNBC from the TCGA database were divided into high- and low-risk groups based on their median risk scores and χ^2 test or Fisher's exact test was used to compare the clinical characteristics of patients with TNBC in different risk groups. Statistical analyses were conducted with R packages (version 4.1.3; RStudio, Inc.). Data matrix construction and data processing were performed using Perl (www.perl.org). Experimental data were analyzed using SPSS (version 29.0; IBM Corp.), while figures were produced using GraphPad Prism (version 8.2.1; Dotmatics). An unpaired t-test was used for comparative assessment of means between two groups, whereas multiple groups were compared using one-way ANOVA followed by Tukey's post-hoc test. All *in vitro* experiments were independently repeated three times. Data are presented as the mean ± standard deviation. $P<0.05$ was considered to indicate a statistically significant difference.

Results

Identification of ferroptosis-related DEGs in the TCGA TNBC cohort. In the present study, 259 genes were determined to be associated with ferroptosis by utilizing the FerrDb website. The ferroptosis-related DEGs across the TNBC and healthy breast samples obtained from the TCGA database were analyzed (Fig. 1A and B). In contrast to the healthy breast tissues, 71 of the 256 ferroptosis-related DEGs (27.7%) varied concerning their expression levels in TNBC samples (34 upregulated and 37 downregulated).

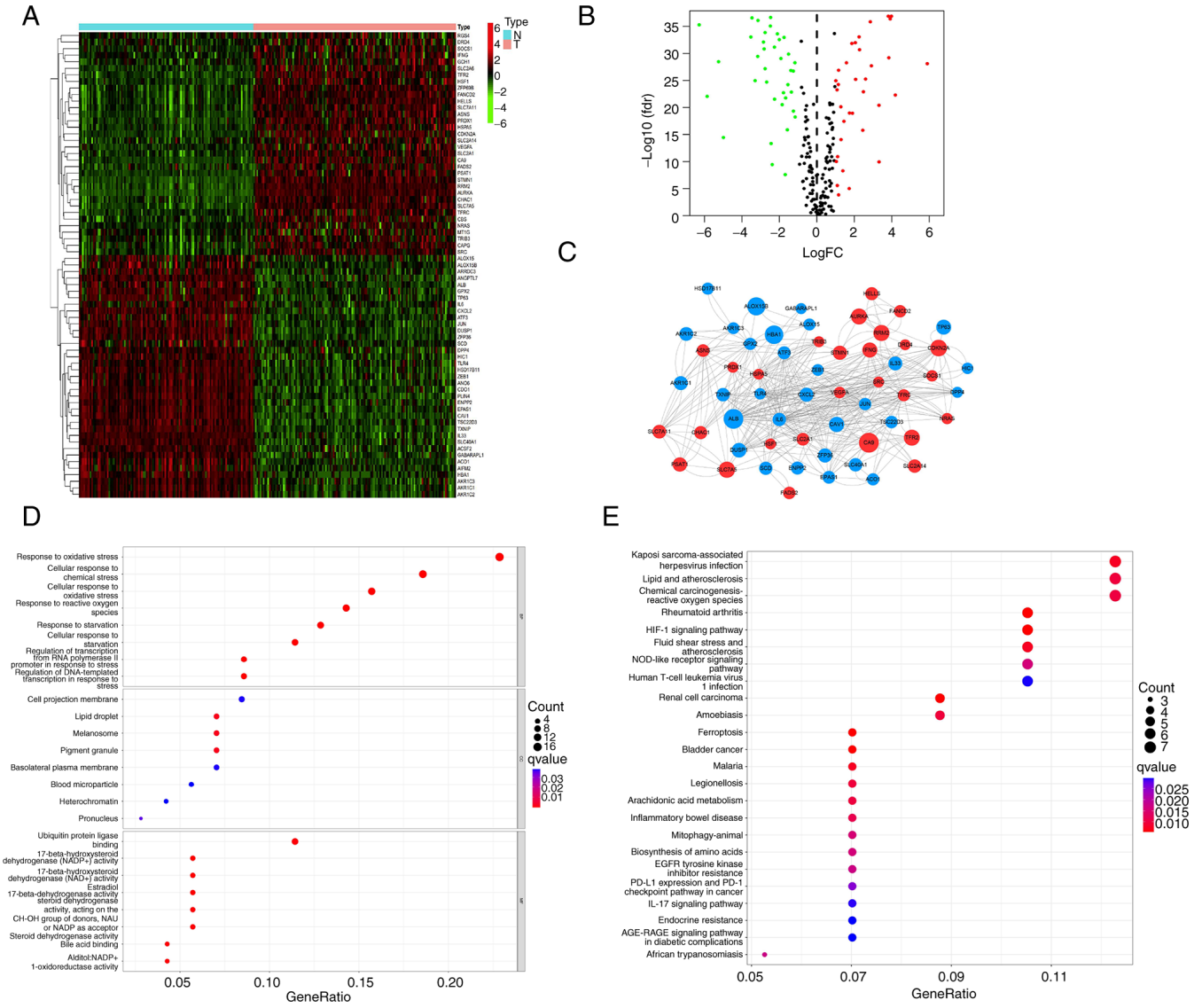

Figure 1. Identification of ferroptosis-related DEGs of TNBC in The Cancer Genome Atlas cohort. (A) Heatmap and (B) volcano plot of the ferroptosis-related DEGs between TNBC and healthy breast tissue. |Log FC|>1 and fdr <0.05. Significantly upregulated and downregulated genes are depicted as red and green dots, respectively. (C) Interactions among candidate genes are shown by the protein-protein interaction network through the Search Tool for the Retrieval of Interacting Genes and proteins database. Results of (D) Gene Ontology biological process enrichment and (E) Kyoto Encyclopedia of Genes and Genomes pathways analysis of DEGs. DEG, differentially expressed gene; TNBC, triple-negative breast cancer; FC, fold change; fdr, false discovery rate.

Furthermore, the protein-protein interaction network of DEGs was established through STRING. Visualization of the detailed regulatory association was achieved through Cytoscape (Fig. 1C). Next, the DEGs were analyzed through GO and KEGG pathway enrichment analyses. GO analysis demonstrated the enrichment of genes involved in several types of oxidative stress functions (Fig. 1D). In addition, KEGG analyses indicated the enrichment of genes involved in ROS-related pathways (Fig. 1E), which were closely associated with ferroptosis.

Prognostic value of ferroptosis-related DEGs. Univariate Cox regression analysis demonstrated that, of the 71 ferroptosis-related DEGs, TFR2, activating transcription factor 3 (ATF3), dual specificity phosphatase 1 (DUSP1)/MAPK phosphatase 1 (MKP-1), regulator of G protein signaling 4 (RGS4) and zinc finger protein 36 (ZFP36) demonstrated prognostic value in TNBC (Fig. 2A). The present study further analyzed the difference in expression levels of ferroptosis-related DEGs with prognostic significance in breast cancer and healthy breast tissue in the HPA database and the results demonstrated that the expression levels of three genes (TFR2, ATF3 and ZFP36) were higher in tumor tissue compared with healthy tissue, which was consistent with the bioinformatics analysis results (Fig. 2B). However, DUSP1 and RGS4 could not be found in the HPA database. Next, the KM Plotter (integrating E-MTAB-365, E-TABM-43 and a series of GEO datasets) was employed to investigate the prognostic significance of these genes in patients with TNBC. Increased expression levels of TFR2, ATF3, RGS4 and ZFP36 were significantly associated with decreased OS in patients with TNBC (Fig. 2C-H). There was no marked association between DUSP1/MKP-1 expression levels and OS (P=0.058).

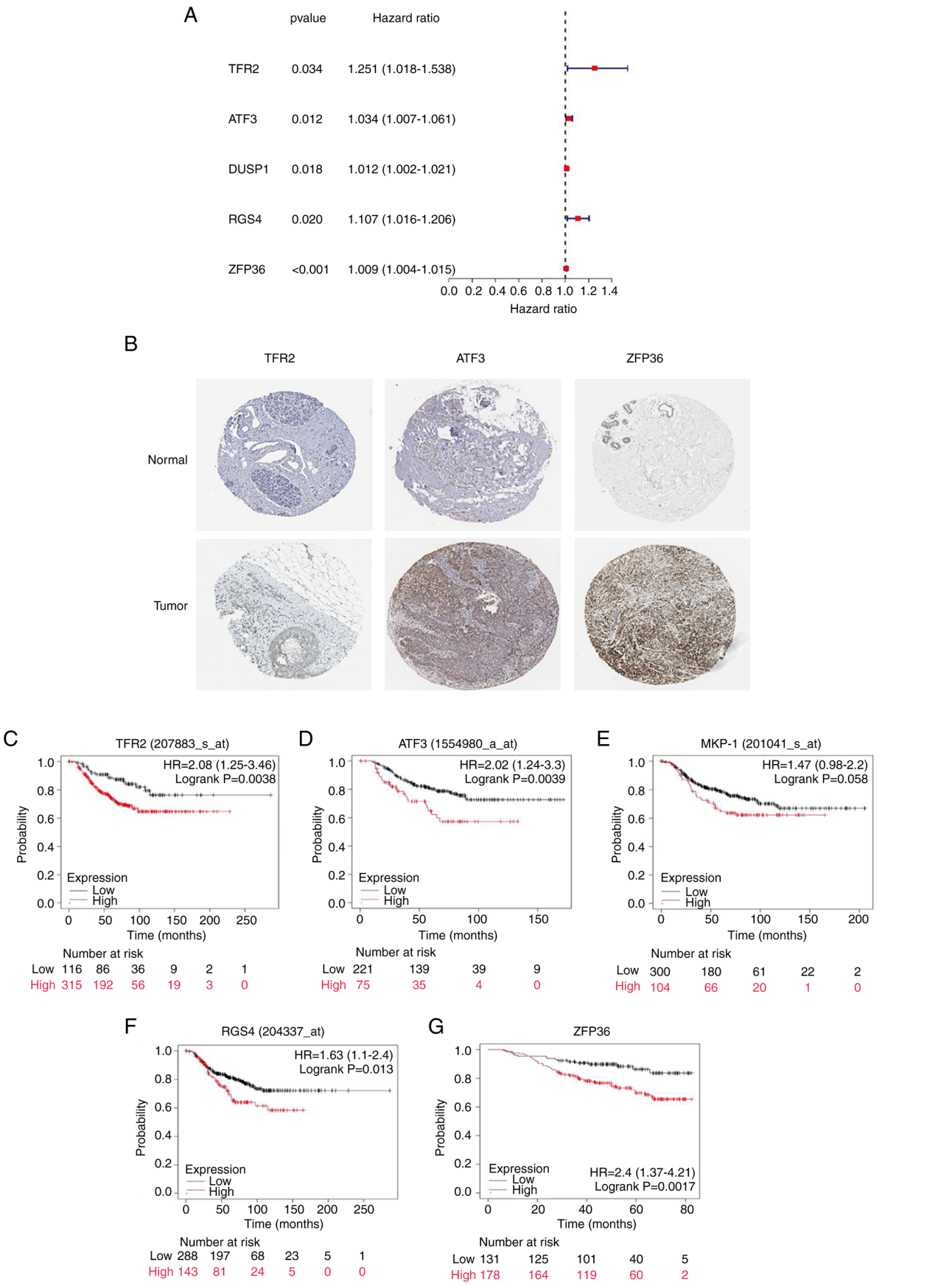

Figure 2. Evaluation of prognostic ferroptosis-related DEGs. (A) A total of five ferroptosis-related genes were identified by univariate Cox regression analysis with prognostic value (95% CI) in triple-negative breast cancer. (B) The expression of TFR2, ATF3 and ZFP36 in healthy breast tissue and breast cancer samples from the Human Protein Atlas database (magnification, x100). Association of the expression levels of ferroptosis-related DEGs with overall survival, including (C) TFR2, (D) ATF3, (E) MKP-1, (F) RGS4 and (G) ZFP36; information in brackets represents gene probes. HR, hazard ratio; TFR2, transferrin receptor 2; ATF3, activating transcription factor 3; MKP-1, MAPK phosphatase 1; DUSP1, dual specificity phosphatase 1; RSG4, regulator of G protein signaling 4; ZFP36, zinc finger protein 36; DEG, differentially expressed gene.

Construction of a three-gene model using TCGA cohort and its validation using the GEO cohort. LASSO Cox regression was performed to establish a prognostic model utilizing the expression of five genes linked to ferroptosis. Calculation of the risk score was performed as follows: Risk score=$e^{(0.279x \text{ TFR2 expression level} + 0.113x \text{ RGS4 expression level} + 0.011x \text{ ZFP36 expression level})}$ (Table SII). Regarding the risk score, a three-gene (TFR2, RGS4 and ZFP36) model was established for the TCGA cohort. Categorization of patients with TNBC into high-risk (n=59) and low-risk (n=59) groups was conducted according to their median risk score and prognostic genes were analyzed (Fig. 3A). Clinical correlation analysis demonstrated that patients with TNBC in the high-risk group exhibited a markedly increased incidence of lymph node metastases and advanced tumor stages (P=0.085 and P=0.086, respectively; Table II). KM curve analysis demonstrated a significantly higher OS in the low-risk group in comparison with the high-risk group in the TCGA dataset (Fig. 3B) and also in the GSE25307 dataset (Fig. 3C). The t-SNE and PCA analyses demonstrated that the individuals in the risk groups were distinctly separated (Fig. 3D). To validate the prognostic significance of the three-gene model, the categorization of individuals with TNBC in the GEO cohort (GSE25307) into risk groups (high and low) was performed according to their median risk score. Similar PCA and t-SNE results were demonstrated in the GEO and TCGA cohorts (Fig. 3E). The respective area under the curve (AUC) values of the three-gene signature model for 1-, 2- and 3-year OS prediction in the TCGA cohort were 0.721, 0.840 and 0.856, respectively, thus indicating a good prognostic value (Fig. 3F). In addition, the respective AUC values of the three-gene signature model for 1-, 3- and 5-year OS prediction in the GSE25307 dataset were 0.615, 0.688 and 0.685, respectively (Fig. 3G). These findings confirmed the adaptability of the aforementioned three-gene model in TNBC.

Evaluation of the independent prognostic value of the three-gene signature. Univariate and multivariate Cox analyses were conducted to examine the risk scores concerning their independent prognostic value in predicting the OS of patients with TNBC. The results indicated the capability of the risk score to function as an independent prognostic factor in univariate [hazard ratio (HR)=1.113; 95% confidence interval (CI)=1.053-1.175; P<0.001] and multivariate (HR=1.111; 95% CI=1.042-1.185; P=0.001) Cox analyses (Fig. 4A and B). In addition, multivariate Cox regression analysis demonstrated that tumor stage could independently function as a prognosis predictor (P=0.007; Fig. 4B).

A heatmap was utilized to demonstrate the link between the expression of genes in the prognostic model and clinical factors (Fig. 4C). Risk score and clinicopathological factors were examined concerning their capacity to predict recurrences of TNBC using an ROC curve. The AUC of the risk score was 0.856, indicative of the improved capability of the risk score in predicting prognosis in comparison with the traditional clinicopathological factors (Fig. 4D). DCA demonstrated that the risk score slightly enhanced the clinical benefit for clinical decisions (Fig. 4E). Furthermore, the 1-, 3- and 5-year OS prediction for individuals with TNBC was carried out by developing a nomogram (Fig. 4F), which enabled improved individualized prognosis.

GSEA and immune-related function based on risk scores in TCGA cohort. To explore the functions and signaling pathways linked to the ferroptosis-related risk signature, DEGs were subjected to GSEA. In low-risk patients, the glutathione metabolism, fructose and mannose metabolism and pentose phosphate pathways were enriched (Fig. 5A-C, respectively). Immunotherapy is an important therapeutic modality for TNBC. Thus, ssGSEA was conducted to explore the association of the risk score with the immune status (Fig. 5D). The expression levels of immune checkpoint molecules were compared across the risk groups and the results demonstrated that TNF superfamily member (TNFSF)18, CD160, adenosine A2a receptor, neuropilin-1, CD200 and TNFSF9 were markedly upregulated, while CD44 was markedly downregulated in the high-risk group compared with the low-risk group (Fig. 5E). These findings demonstrated potential ferroptosis-related metabolic pathways and immunotherapeutic targets of TNBC.

TFR2 knockdown inhibits the proliferation of TNBC cells. Previous studies have documented the role of RGS4 and ZFP36 in breast cancer (19,20). Thus, the current study focused on the previously unreported involvement of TFR2 in TNBC. The expression level of TFR2 in healthy breast epithelial cells and breast cancer cell lines was examined. RT-qPCR analysis demonstrated that the TFR2 mRNA levels were downregulated in healthy and ER-positive breast cancer cells and upregulated in ER-negative breast cancer cell lines, particularly in TNBC cell lines (Fig. 6A). The TNBC cell line MDA-MB-436 was subjected to further analyses, as it exhibited the highest TFR2 mRNA expression levels. TFR2 was knocked down in MDA-MB-436 cells using siRNA and si-TFR2 1# was selected for further experiments, as it exhibited the highest knockdown efficiency (Fig. 6B). The mRNA and protein expression levels of TFR2 in the si-TFR2-transfected group were significantly reduced compared with the NC group (P<0.05; Fig. 6C). Next, the cell viability impact of knocking down TFR2 was examined in MDA-MB-436 cells by the CCK-8 assay. TFR2 knockdown significantly suppressed the proliferation of MDA-MB-436 cells at 24, 48 and 72 h post-transfection (P<0.01; Fig. 6D). These data suggested that TFR2 may function as an oncogenic factor, which was in agreement with the data acquired through bioinformatics analyses.

TFR2 knockdown promotes ferroptosis in TNBC cells. The impact of TFR2 knockdown on ferroptosis in MDA-MB-436 cells was examined. Lipid peroxidation is one of the characteristics of cellular ferroptosis; therefore, the levels of lipid peroxidation in MDA-MB-436 cells were examined by analyzing the MDA levels. TFR2 knockdown significantly increased the MDA levels in MDA-MB-436 cells (P<0.01; Fig. 6E), which suggested that the induction of ferroptosis had occurred. Next, the protein expression levels of ferroptosis-related factors were assessed through western blotting. Compared with the NC group, the LOX protein expression levels were significantly elevated, whereas the SLC7A11, GPX4 and FTH1 levels were significantly reduced in the si-TFR2 transfected group (P<0.01; Fig. 6F), which further demonstrated the induction of ferroptosis. Next, the effect of 0.5 μM ferrostatin-1 on the proliferation of MDA-MB-436 cells was examined using a CCK-8 assay. Ferrostatin-1

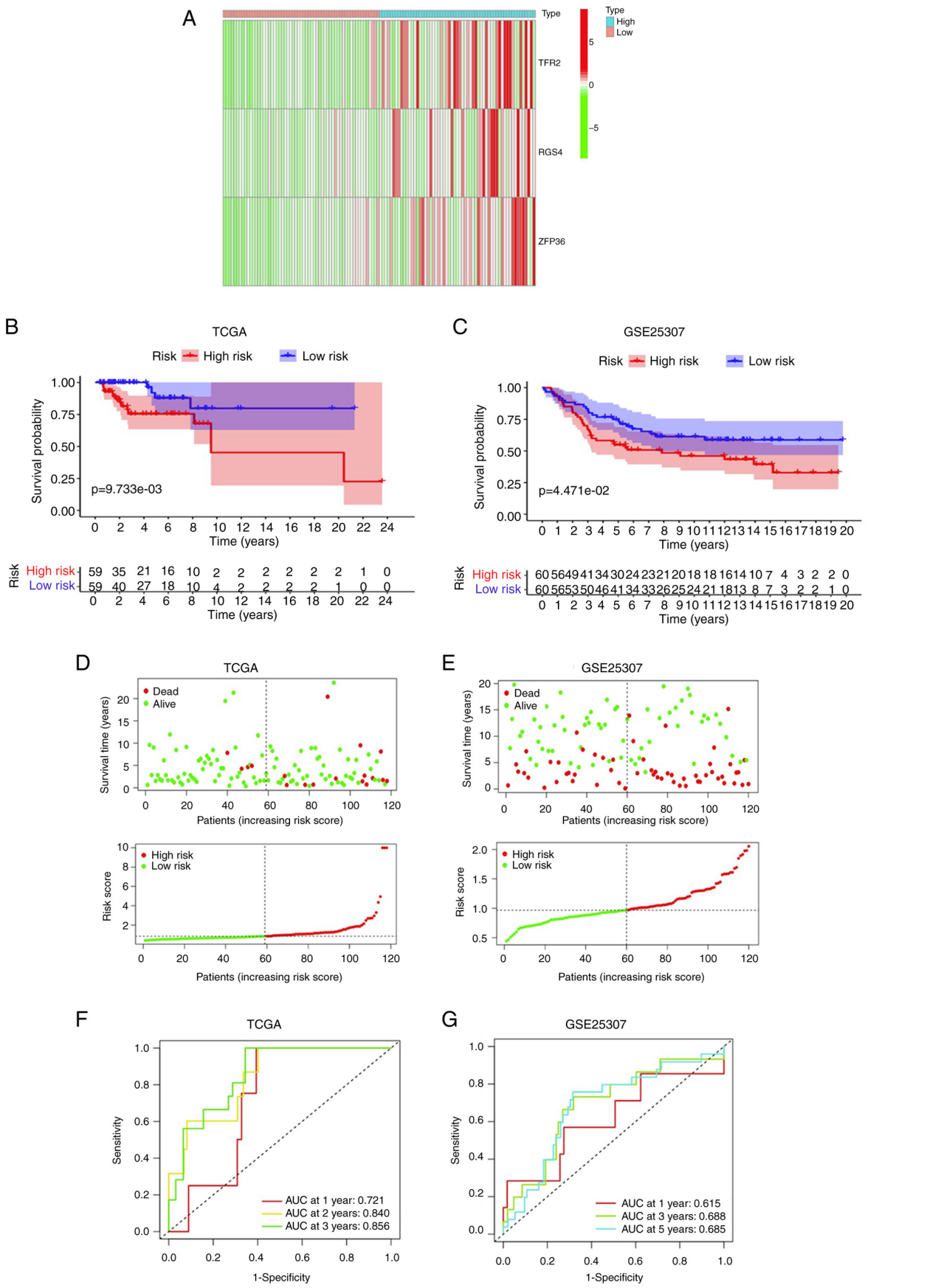

Figure 3. Construction and validation of a three-gene model based on least absolute shrinkage and selection operator Cox regression analysis. (A) Heatmap showing the expression of three genes in different risk groups of patients with triple-negative breast cancer according to the risk score in the TCGA cohort. Kaplan-Meier survival curves of the overall survival of high-risk and low-risk groups in (B) TCGA and (C) GEO (GSE25307) datasets (95% CI). The distribution of the risk scores and the relationship between survival time, survival status and risk scores in (D) TCGA and (E) GEO (GSE25307) datasets. The areas under the curve of time-dependent receiver operating characteristic curves for the three-gene signature in the (F) TCGA and (G) GEO (GSE25307) cohorts. TCGA, The Cancer Genome Atlas; GEO, Gene Expression Omnibus; AUC, area under the curve.

Table II. Comparison of clinical characteristics in low- and high-risk groups based on The Cancer Genome Atlas cohort.

Characteristics	Low-risk group (n=59)	High-risk group (n=59)	P-value
Age, years			0.843
≤60	41 (69.5)	40 (67.8)	
>60	18 (30.5)	19 (32.2)	
T stage			0.387
T1	9 (15.3)	19 (32.2)	
T2	40 (15.3)	34 (57.6)	
T3	9 (67.8)	3 (5.1)	
T4	0 (0)	3 (5.1)	
Unknown	1 (1.6)		
N stage			0.085
N0	42 (71.2)	33 (55.9)	
N1	13 (22.0)	16 (27.1)	
N2	2 (3.4)	6 (10.2)	
N3	2 (3.4)	4 (6.8)	
M stage			0.496[a]
M0	54 (91.5)	55 (93.2)	
M1	0 (0)	2 (3.4)	
Unknown	5 (8.5)	2 (3.4)	
Tumor stage			0.086
I	9 (15.3)	11 (18.6)	
II	42 (71.2)	34 (57.6)	
III	6 (10.1)	11 (18.6)	
IV	0 (0)	2 (3.5)	
Unknown	2 (3.4)	1 (1.7)	

[a]Fisher's exact test. Values are expressed as n (%).

significantly reversed the decrease in cell viability induced by TFR2 as compared with the si-TFR2 transfected cells (P<0.05; Fig. 6G). The resulting data were indicative of the suppressive impact of TFR2 on the viability of TNBC cells by inducing ferroptosis.

Discussion

It was recently reported that ferroptosis induction may act as a promising treatment strategy for breast cancer (21). A previous study highlighted the role of both experimental compounds and clinical drugs in inducing ferroptosis in breast cancer cells (22). TNBC, the most malignant subtype of breast cancer, was previously reported to be intrinsically sensitive to ferroptosis due to its non-apoptotic characteristics. The therapeutic effects of a number of types of ferroptosis inducers on TNBC have been previously evaluated (12,23). Erastin, the most widely used ferroptosis inducer, increases the sensitivity of TNBC cells to ferroptosis by upregulating mitochondrial ROS (24). However, the application of erastin is limited due to its potentially serious side effects, such as nephrotoxicity (25). A recent study reported that the ferroptosis inducer 18-β-glycyrrhetinic acid promoted the death of TNBC cells through the upregulation of peroxidation (26). However, the association between genes related to ferroptosis with TNBC and potential biomarkers of ferroptosis in TNBC has not been completely elucidated to date.

In contrast to a single biomarker-based signature, a multigene signature model is more accurate for predicting the prognosis of patients with breast cancer. For instance, Oncotype Dx® (21-gene signature) and Mammaprint (70-gene signature) have been widely used in the clinic to evaluate the favorable impact of chemotherapy in patients with luminal-type breast cancer (27). A number of preliminary studies have explored the functions of genes linked to ferroptosis in breast cancer using a multigene signature model (16,22,28,29). However, the involvement of these regulators in TNBC remains to be elucidated. In the present study, 259 genes linked to ferroptosis were retrieved from the FerrDb website and a systematic exploration of the expression levels of these genes in TNBC was conducted. Of these 259 genes, 60 (23.4%) varied in expression levels across TNBC and healthy breast tissues. GO and KEGG analyses demonstrated the enrichment of these DEGs in several ROS-related pathways, which are among the main mediators of ferroptosis. Univariate Cox analysis demonstrated an association of five DEGs with OS of patients with TNBC. Upregulation of these five genes was associated with poor prognosis. To further verify these results, KM Plotter was utilized for examining the association between these genes and prognosis of

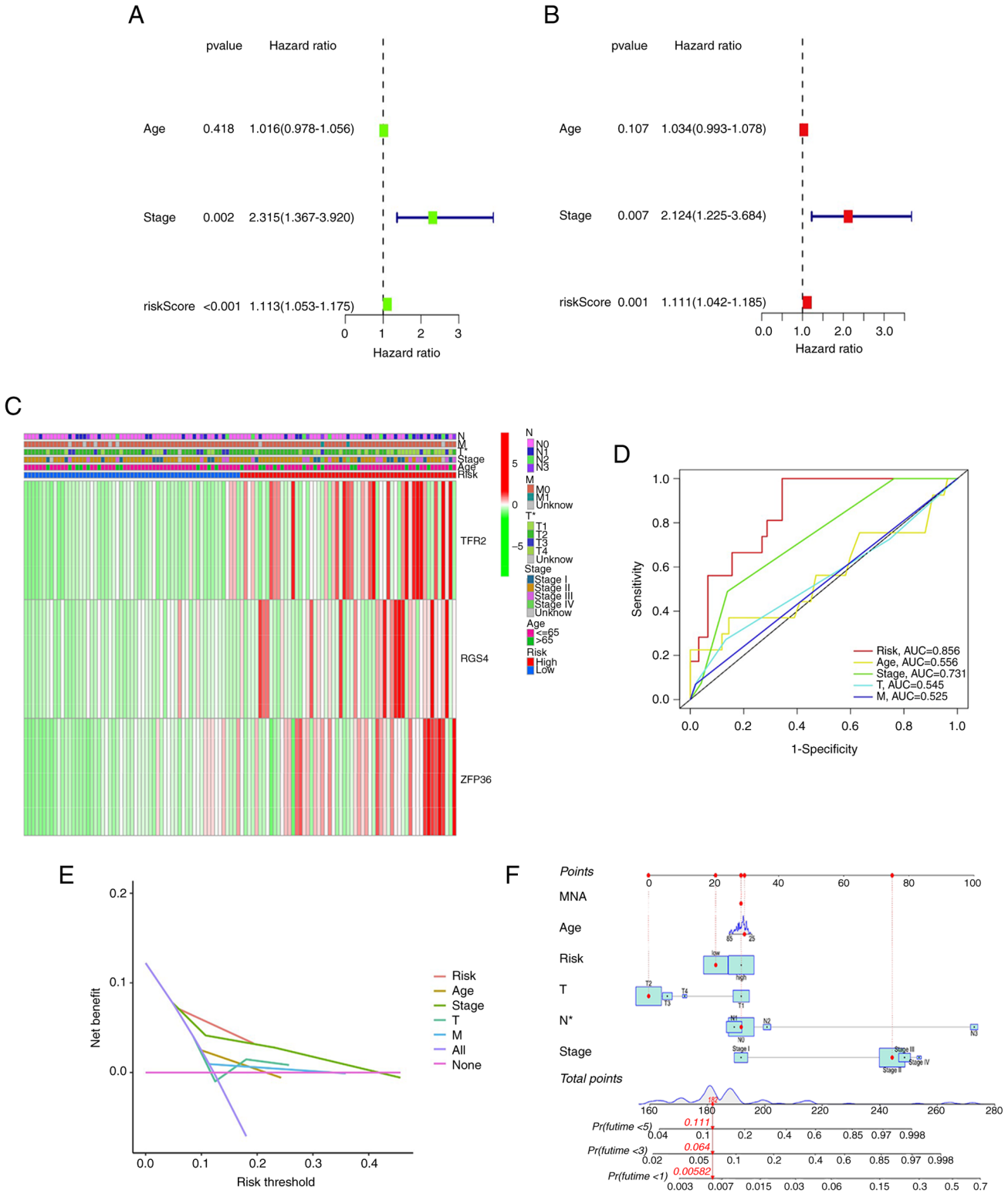

Figure 4. Relationship between risk scores and clinicopathological factors in TNBC. Forest plots of the prognostic role of risk scores in predicting overall survival of TNBC as examined using (A) univariate and (B) multivariate Cox regression analyses (95% CI). (C) Heatmap of the distribution of ferroptosis-related gene expression and clinical factors. (D) Comparison of the risk scores with traditional clinicopathological factors in the prognostic prediction based on the receiver operating characteristic curve analysis. (E) Decision curve analysis comparing the net survival benefit of the risk scores with clinicopathological factors (red represents upregulation and green represents downregulation). (F) Nomogram used to predict prognosis based on the risk scores and clinicopathological factors. TNBC, triple-negative breast cancer; TFR2, transferrin receptor 2; RSG4, regulator of G protein signaling 4; ZFP36, zinc finger protein 36; AUC, area under the curve; T, tumor size; N, lymph node metastasis; MNA, distant metastasis; Pr, survival probability.

TNBC. Upregulation of these five genes was associated with decreased OS. The resulting data suggested that ferroptosis may serve a role in the pathogenesis of TNBC.

Next, a prognostic model was established using LASSO Cox regression. It comprised three ferroptosis-related genes (TFR2, RGS4 and ZFP36). High- and low-risk categories of

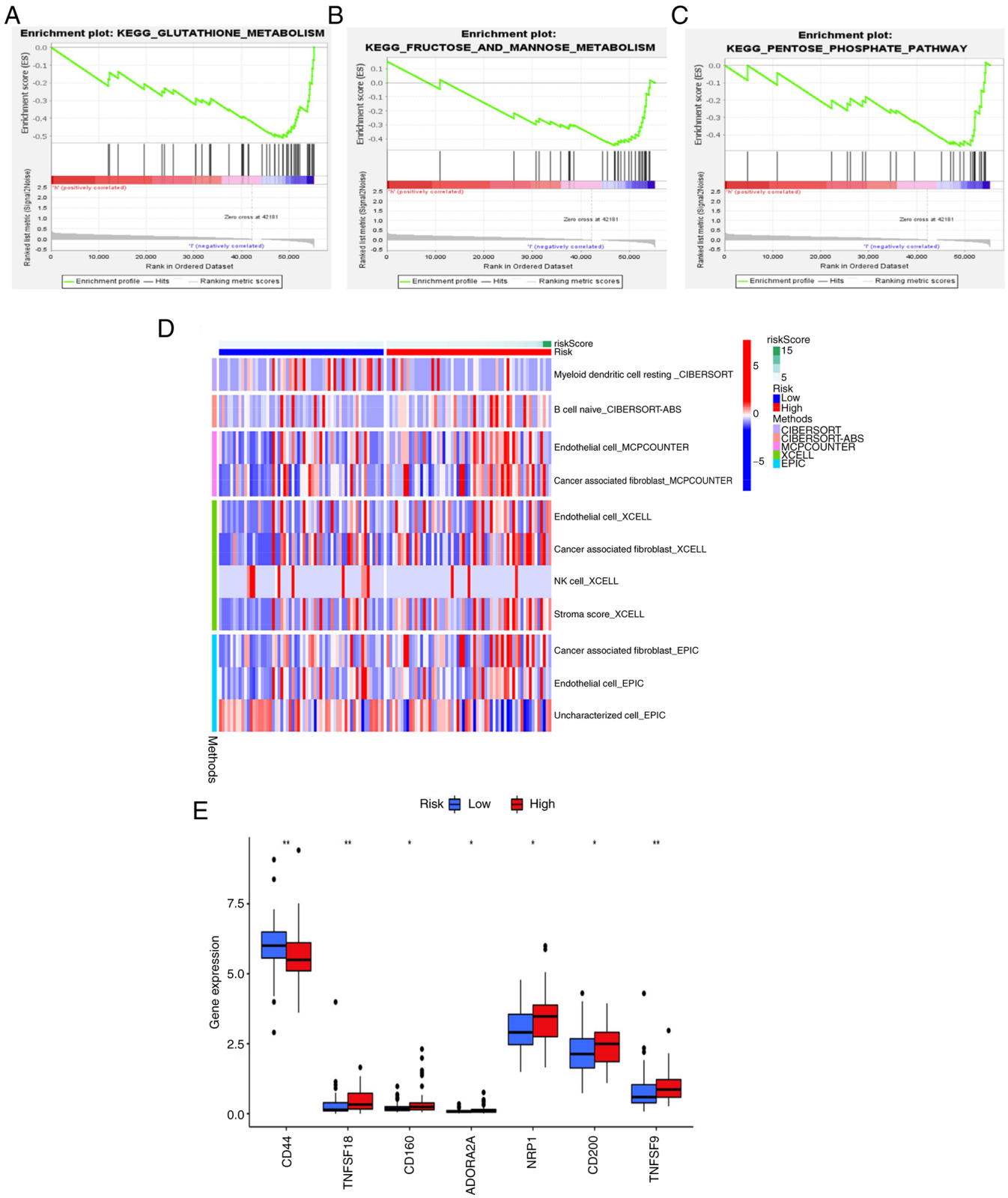

Figure 5. Risk score of ferroptosis-related gene models is closely related to metabolic and immune function in triple-negative breast cancer. GSEA of the associated (A) glutathione metabolism, (B) fructose and mannose metabolism and (C) pentose phosphate signaling pathways in the low-risk group. (D) Heatmap of the correlation between risk score and immune status was explored by ssGSEA. (E) The differences in the expression levels of immune check-point molecules between the high- and low-risk score groups. *P<0.05; **P<0.01 vs. low risk. GSEA, gene set enrichment analysis; ssGSEA, single-sample GSEA; KEGG, Kyoto Encyclopedia of Genes and Genomes; TNFS, TNF superfamily member; ADORA2A, adenosine A2a receptor; NRP1, neuropilin-1.

patients with TNBC were established with subsequent categorization performed according to their median risk score. KM and ROC curves were employed to validate the prognostic value of the model. Analysis of risk scores in combination with clinical factors indicated the capability of the risk score to independently predict survival. The model demonstrated

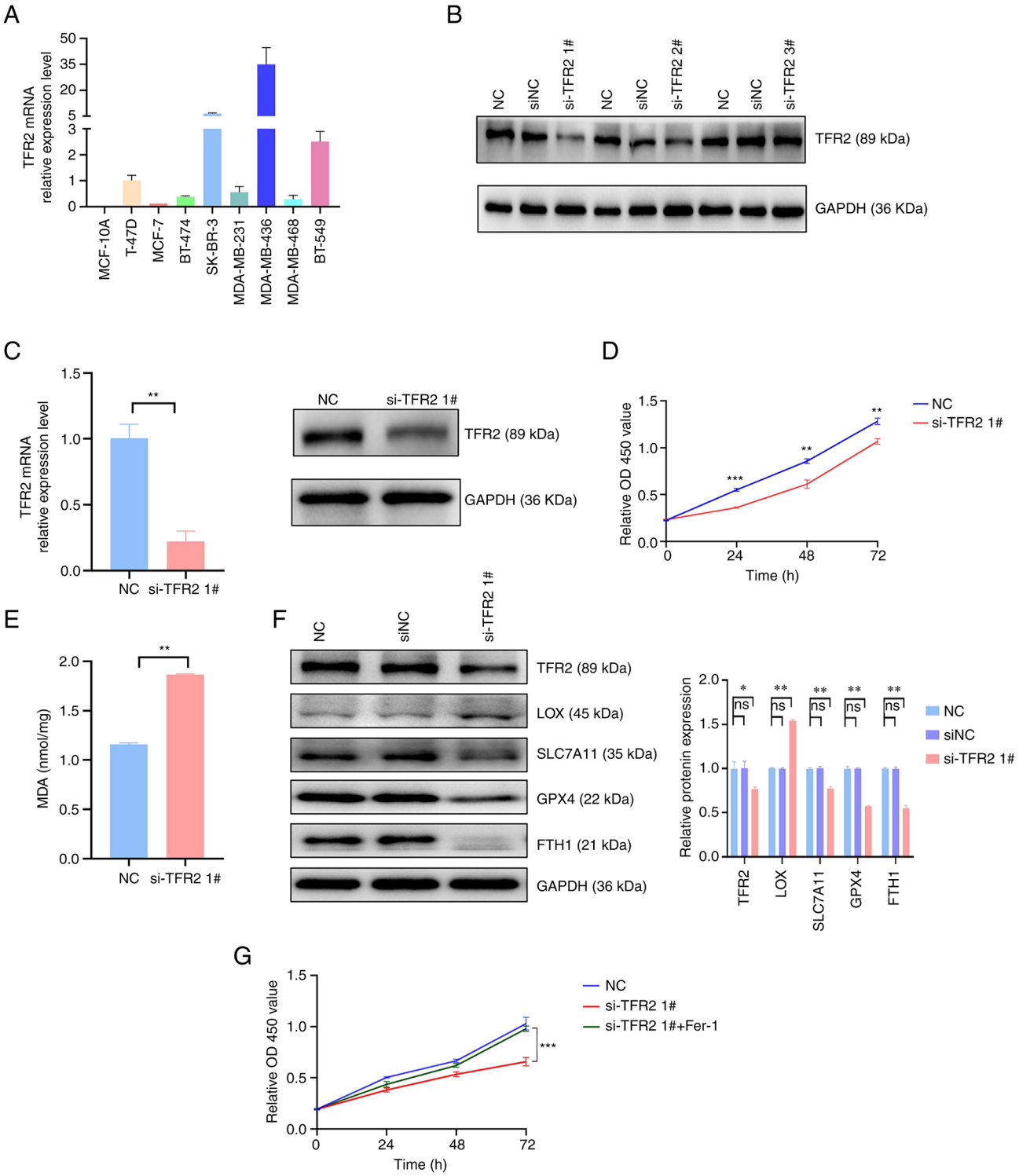

Figure 6. Knockdown of TFR2 promotes ferroptosis in the triple-negative breast cancer cell line MDA-MB-436. (A) The expression levels of TFR2 were detected by reverse transcription-quantitative PCR in healthy breast and breast cancer cell lines. (B) Western blot analysis of si-TFR2 knockdown efficiency. (C) Relative changes in the mRNA and protein expression levels of TFR2 in MDA-MB-436 cells after transfection with siRNA. (D) Cell viability of MDA-MB-436 cells was analyzed by a CCK-8 assay at 0, 24, 48 and 72 h after knockdown of TFR2 with siRNA. (E) Relative changes of MDA levels in MDA-MB-436 cells after knockdown of TFR2 compared with negative controls. (F) The expression levels of ferroptosis-related proteins were analyzed by western blot. (G) The viability of MDA-MB-436 cells was determined using a CCK-8 assay at 0, 24, 48 and 72 h after transfection with siRNA with or without 0.5 μM ferrostatin-1 treatment. Values are expressed as the mean ± standard deviation (n=3 independent experiments). *P<0.05, **P<0.01 and ***P<0.001 vs. NC. CCK-8, cell counting kit-8; OD, optical density; TFR2, transferrin receptor 2; NC, negative control; si, short interfering; MDA, malondialdehyde; LOX, lysyl oxidase; SLC7A11, solute carrier family 7 member 11; GPX4, glutathione peroxidase 4; FTH1, ferritin heavy chain 1; ns, not significant.

elevated AUC values concerning the 1-, 3- and 5-year survival prediction relative to the clinical model values. DCA analysis demonstrated that the model may be able to increase clinical benefits for treatment decisions. The present study also developed a nomogram, which may aid the 1-, 3- and 5-year OS prediction of patients with TNBC. Furthermore, validation

of the prognostic value of the model was performed utilizing the GSE25307 dataset. These findings demonstrated that this model is able to predict the prognosis of individuals with TNBC.

The prognostic model utilized in the current research comprised three genes linked to ferroptosis, namely TFR2, RGS4 and ZFP36. To the best of our knowledge, the present study was the first to report the combination of these genes as a prognostic signature for TNBC. RGS4, a maker of ferroptosis (30), regulates the activity of G-protein-coupled receptors in various types of tumor cell (31,32), including breast cancer (19). Previous research has reported that RGS4 overexpression suppresses the proliferation of human breast cancer cells by proteasome degradation (33). Yau *et al* (34) reported that RGS4 is one of the prognostic indicators of early TNBC, thus supporting the findings of the current study. Furthermore, ZFP36, an RNA-binding protein, regulates mRNA stability and suppresses ferroptosis. Previous studies have reported that noncoding RNAs can combine with ZFP36 to modulate the proliferative and migratory capacities of breast cancer cells (35,36). Dong *et al* (37) reported that ZFP36 promoted the tumorigenesis and progression of breast cancer. TFR2, a driver of ferroptosis, promotes cellular iron transport. A previous study reported that TFR2 is present in ~26% of colon cancer types (38). Furthermore, TFR2 regulated the cell cycle of colon cancer cells utilizing the ERK pathway (39). In addition, downregulation of TFR2 in gastric cancer tissue suggested that the expression of TFR2 was linked to the survival of patients with gastric cancer (40). To date, no studies have been conducted on the potential association between TFR2 and breast cancer. In the present study, the function of TFR2 in TNBC was examined through *in vitro* experiments. TFR2 expression in TNBC cells was upregulated compared with that in healthy breast epithelial and ER-positive breast cancer cells. In addition, TFR2 was demonstrated to exert oncogenic effects in TNBC. It was noted that TFR2 knockdown inhibited TNBC cell proliferation by inducing ferroptosis. To the best of our knowledge, the current study appears to be the first to report the role of TFR2 in TNBC. Thus, TFR2-induced ferroptosis may be a potential future treatment target for TNBC. However, further research is warranted to fully understand the specific mechanisms via which TFR2 functions in TNBC. Of note, in the univariate Cox analysis of the present study, the HR value of ZFP36 was low and the HR value of DUSP1 was also similar. The possible reason for the aforementioned results may be that the TNBC sample size of the present study was limited. In addition, in the three-gene model, differences in HR values may also indicate differences in the predictive value of each gene and the effect of TFR2 with the highest HR value on TNBC proliferation was verified through *in vitro* experiments. Further large-sample analyses and functional experiments may explain the aforementioned results.

Immunotherapy can be used for the treatment of aggressive malignancies, including TNBC, which often exhibit resistance to conventional treatment strategies (4,41). Immunotherapies, such as immune checkpoint inhibitors (ICIs) (such as cytotoxic T-lymphocyte-associated protein 4 and programmed cell death protein 1/programmed death-ligand 1) have yielded positive results in clinical practice (42). However, the therapeutic effect of ICIs is limited, as only one-third of cancer patients show a response to these agents. For instance, the KEYNOTE-086 study reported that 21.4% of individuals with TNBC responded to pembrolizumab (43). Prior research has reported that ferroptosis participates in the remodeling of the tumor immune microenvironment and has suggested the importance of identifying novel immunotherapy targets for TNBC (44). Therefore, the present study examined the association of the risk score with the immune status. A total of five immune algorithms were used to examine the relative infiltration levels of immune cells in the samples evaluated. The expression levels of immune checkpoint molecules (CD44, TNFSF18 and NRP1) varied across the risk groups (high- and low-). Thus, these molecules may hold promise as possible immunotherapeutic targets for TNBC.

Recently, Wu *et al* (45) reported ferroptosis-related gene signatures in TNBC. The authors established a 15-ferroptosis-related gene prognostic model using LASSO Cox regression and TCGA datasets. The levels of certain immune cells varied across different risk groups in TNBC. Compared with the study by Wu *et al* (45), the current study has revealed novel findings. In addition to establishing a ferroptosis-related prediction model using a TCGA dataset, the performance of the model was verified using GEO datasets, which markedly increased the reliability of the findings. In addition, the present model determined the differential expression levels of immune checkpoint molecules, thus suggesting novel potential immunotherapeutic targets for TNBC. Furthermore, the data acquired from bioinformatics analyses were confirmed through *in vitro* assays. However, the current study has various limitations. For instance, only data from public databases were used in the present study. In addition, limited *in vitro* experiments were performed. Thus, additional biological assays and clinical analyses must be performed to confirm these results. Furthermore, some important genes may be excluded because the model was developed utilizing genes linked to ferroptosis.

In conclusion, in the present study, a new predictive signature of three ferroptosis-related genes was established for accurately predicting TNBC prognosis, which may be used as a tool for clinical applications. The model developed revealed the differential expression of immune checkpoint molecules, providing useful insight into the identification of treatment targets for TNBC. Furthermore, the present study demonstrated that TFR2 negatively regulated ferroptosis in TNBC. Additional studies are required to elucidate the role of TFR2 in TNBC in the future.

Acknowledgements

Not applicable.

Funding

The present study was supported by grants from the National Natural Science Foundation of China (grant no. NSFC 82160484), Guizhou Province Science Plan Program [Qian Ke He Foundation-ZK (2022) general; grant no. 640] and Zunyi Science and Technology Project [Zunshi Kehe Hz Zi (2022); grant no. 295].

Availability of data and materials

The data used in the present study are publicly available from the TCGA (http://cancergenome.nih.gov/), GEO (https://www.ncbi.nlm.nih.gov/geo/), FerrDb (http://www.zhounan.org/ferrdb/), STRING (https://string-db.org) and Kaplan-Meier Plotter (http://kmplot.com/analysis). The datasets used and/or analyzed during the current study are available from the corresponding author on reasonable request.

Authors' contributions

YY and RC designed the study. RC and JD prepared the original draft of the manuscript. YY and JD performed the experiments. YY and JD confirm the authenticity of all the raw data. YFH, WH, LL and DL analyzed the results. YY, RC and JD designed the tables and figures. RC and YY revised the final manuscript. All authors have read and approved the final version of the manuscript.

Ethics approval and consent to participate

Not applicable.

Patient consent for publication

Not applicable.

Competing interests

The authors declare that they have no competing interests.

References

1. Siegel RL, Miller KD, Fuchs HE and Jemal A: Cancer statistics, 2022. CA Cancer J Clin 72: 7-33, 2022.
2. Waks AG and Winer EP: Breast cancer treatment: A review. JAMA 321: 288-300, 2019.
3. Sharma M, Turaga RC, Yuan Y, Satyanarayana G, Mishra F, Bian Z, Liu W, Sun L, Yang J and Liu ZR: Simultaneously targeting cancer-associated fibroblasts and angiogenic vessel as a treatment for TNBC. J Exp Med 218: e20200712, 2021.
4. Marra A, Viale G and Curigliano G: Recent advances in triple negative breast cancer: The immunotherapy era. BMC Med 17: 90, 2019.
5. Yu B, Luo F, Sun B, Liu W, Shi Q, Cheng SY, Chen C, Chen G, Li Y and Feng H: KAT6A Acetylation of SMAD3 regulates Myeloid-derived suppressor cell recruitment, metastasis, and immunotherapy in Triple-Negative breast cancer. Adv Sci (Weinh) 8: e2100014, 2021.
6. Gao W, Wang X, Zhou Y, Wang X and Yu Y: Autophagy, ferroptosis, pyroptosis, and necroptosis in tumor immunotherapy. Signal Transduct Target Ther 7: 196, 2022.
7. Yao Y, Shi Y, Gao Z, Sun Y, Yao F and Ma L: Ferroptosis at the crossroads of tumor-host interactions, metastasis, and therapy response. Am J Physiol Cell Physiol 323: C95-C103, 2022.
8. Sui S, Xu S and Pang D: Emerging role of ferroptosis in breast cancer: New dawn for overcoming tumor progression. Pharmacol Ther 232: 107992, 2022.
9. Singh T, Beatty A and Peterson JR: The AMPK-related kinase NUAK2 suppresses glutathione peroxidase 4 expression and promotes ferroptotic cell death in breast cancer cells. Cell Death Discov 8: 253, 2022.
10. Sha R, Xu Y, Yuan C, Sheng X, Wu Z, Peng J, Wang Y, Lin Y, Zhou L, Xu S, *et al*: Predictive and prognostic impact of ferroptosis-related genes ACSL4 and GPX4 on breast cancer treated with neoadjuvant chemotherapy. EBioMedicine 71: 103560, 2021.
11. Xu G, Wang H, Li X, Huang R and Luo L: Recent progress on targeting ferroptosis for cancer therapy. Biochem Pharmacol 190: 114584, 2021.
12. Doll S, Proneth B, Tyurina YY, Panzilius E, Kobayashi S, Ingold I, Irmler M, Beckers J, Aichler M, Walch A, *et al*: ACSL4 dictates ferroptosis sensitivity by shaping cellular lipid composition. Nat Chemical Biol 13: 91-98, 2017.
13. Timmerman LA, Holton T, Yuneva M, Louie RJ, Padró M, Daemen A, Hu M, Chan DA, Ethier SP, van 't Veer LJ, *et al*: Glutamine sensitivity analysis identifies the xCT antiporter as a common triple-negative breast tumor therapeutic target. Cancer Cell 24: 450-465, 2013.
14. Chen PH, Wu J, Ding CC, Lin CC, Pan S, Bossa N, Xu Y, Yang WH, Mathey-Prevot B and Chi JT: Kinome screen of ferroptosis reveals a novel role of ATM in regulating iron metabolism. Cell Death Differ 27: 1008-1022, 2020.
15. Tang X, Ding CK, Wu J, Sjol J, Wardell S, Spasojevic I, George D, McDonnell DP, Hsu DS, Chang JT and Chi JT: Cystine addiction of triple-negative breast cancer associated with EMT augmented death signaling. Oncogene 36: 4379, 2017.
16. Zhu L, Tian Q, Jiang S, Gao H, Yu S, Zhou Y, Yan Y, Ren Y, He J and Wang B: A novel Ferroptosis-Related gene signature for overall survival prediction in patients with breast cancer. Front Cell Dev Biol 9: 670184, 2021.
17. Győrffy B: Survival analysis across the entire transcriptome identifies biomarkers with the highest prognostic power in breast cancer. Comput Struct Biotechnol J 19: 4101-4109, 2021.
18. Livak KJ and Schmittgen TD: Analysis of relative gene expression data using real-time quantitative PCR and the 2(-Delta Delta C(T)) method. Methods 25: 402-408, 2001.
19. Xie Y, Wolff DW, Wei T, Wang B, Deng C, Kirui JK, Jiang H, Qin J, Abel PW and Tu Y: Breast cancer migration and invasion depend on proteasome degradation of regulator of G-protein signaling 4. Cancer Res 69: 5743-5751, 2009.
20. Pan QH, Fan YH, Wang YZ, Li DM, Hu CE and Li RX: Long noncoding RNA NNT-AS1 functions as an oncogene in breast cancer via repressing ZFP36 expression. J Biol Regul Homeost Agents 34: 795-805, 2020.
21. Li D, Zhang J and Zhao X: Mechanisms and molecular targets of artemisinin in cancer treatment. Cancer Invest 39: 675-684, 2021.
22. Peng Y, Yu H, Zhang Y, Qu F, Tang Z, Qu C, Tian J, Zong B, Wang Y, Ren H and Liu S: A ferroptosis-associated gene signature for the prediction of prognosis and therapeutic response in luminal-type breast carcinoma. Sci Rep 11: 17610, 2021.
23. Al-Taie Z, Hannink M, Mitchem J, Papageorgiou C and Shyu CR: Drug repositioning and subgroup discovery for precision medicine implementation in triple negative breast cancer. Cancers (Basel) 13: 6278, 2021.
24. Dixon SJ, Lemberg KM, Lamprecht MR, Skouta R, Zaitsev EM, Gleason CE, Patel DN, Bauer AJ, Cantley AM, Yang WS, *et al*: Ferroptosis: An Iron-dependent form of nonapoptotic cell death. Cell 149: 1060-1072, 2012.
25. Liao M, Qin R, Huang W, Zhu HP, Peng F, Han B and Liu B: Targeting regulated cell death (RCD) with small-molecule compounds in triple-negative breast cancer: A revisited perspective from molecular mechanisms to targeted therapies. J Hematol Oncol 15: 44, 2022.
26. Wen Y, Chen H, Zhang L, Wu M, Zhang F, Yang D, Shen J and Chen J: Glycyrrhetinic acid induces oxidative/nitrative stress and drives ferroptosis through activating NADPH oxidases and iNOS, and depriving glutathione in Triple-Negative breast cancer cells. Free Radic Biol Med 173: 41-51, 2021.
27. Oliveira LJC, Amorim LC, Megid TBC, de Resende CAA and Mano MS: Gene expression signatures in early breast cancer: Better together with clinicopathological features. Crit Rev Oncol Hematol 175: 103708, 2022.
28. Wu ZH, Tang Y, Yu H and Li HD: The role of ferroptosis in breast cancer patients: A comprehensive analysis. Cell Death Discov 7: 93, 2021.
29. Tang W, Xu F, Zhao M and Zhang S: Ferroptosis regulators, especially SQLE, play an important role in prognosis, progression and immune environment of breast cancer. BMC Cancer 21: 1160, 2021.
30. Stockwell BR: Ferroptosis turns 10: Emerging mechanisms, physiological functions, and therapeutic applications. Cell 185: 2401-2421, 2022.
31. Guda MR, Velpula KK, Asuthkar S, Cain CP and Tsung AJ: Targeting RGS4 Ablates Glioblastoma proliferation. Int J Mol Sci 21: 3300, 2020.
32. Hu Y, Zheng M, Wang S, Gao L, Gou R, Liu O, Dong H, Li X and Lin B: Identification of a five-gene signature of the RGS gene family with prognostic value in ovarian cancer. Genomics 113: 2134-2144, 2021.

33. Park HJ, Kim SH and Moon DO: Growth inhibition of human breast carcinoma cells by overexpression of regulator of G-protein signaling 4. Oncol Lett 13: 4357-4363, 2017.
34. Yau C, Esserman L, Moore DH, Waldman F, Sninsky J and Benz CC: A multigene predictor of metastatic outcome in early stage hormone receptor-negative and triple-negative breast cancer. Breast Cancer Res 12: R85, 2010.
35. Ding Y, Li Y, Duan Y, Wang W, Zheng W, Cheng W, Qi Y, Feng J, Chen Z, Yu T, *et al*: LncRNA MBNL1-AS1 represses proliferation and cancer Stem-Like properties of breast cancer through MBNL1-AS1/ZFP36/CENPA Axis. J Oncol 2022: 9999343, 2022.
36. Fang S, Zhao Y and Hu X: LncRNA ADAMTS9-AS1 restrains the aggressive traits of breast carcinoma cells via sponging miR-513a-5p. Cancer Manag Res 12: 10693-10703, 2020.
37. Dong X, Yang Y, Xu G, Tian Z, Yang Q, Gong Y and Wu G: The initial expression alterations occurring to transcription factors during the formation of breast cancer: Evidence from bioinformatics. Cancer Med 11: 1371-1395, 2022.
38. Calzolari A, Deaglio S, Maldi E, Cassoni P, Malavasi F and Testa U: TfR2 expression in human colon carcinomas. Blood Cells Mol Dis 43: 243-249, 2009.
39. Calzolari A, Larocca LM, Deaglio S, Finisguerra V, Boe A, Raggi C, Ricci-Vitani L, Pierconti F, Malavasi F, De MariaR, *et al*: Transferrin receptor 2 is frequently and highly expressed in glioblastomas. Transl Oncol 3: 123-134, 2010.
40. Zhao QF, Ji J, Cai Q, Wang C, Shi M, Zhou CF, Zhu ZG and Zhang J: Low expression of transferrin receptor 2 predict poor prognosis in gastric cancer patients. Kaohsiung J Med Sci 36: 1014-1020, 2020.
41. Cao Y, Chen C, Tao Y, Lin W and Wang P: Immunotherapy for Triple-Negative Breast Cancer. Pharmaceutics 13: 2003, 2021.
42. Xu X, Wang D, Chen W, Li N, Suwinski R, Rossi A, Rosell R, Zhong J and Fan Y: A nomogram model based on peripheral blood lymphocyte subsets to assess the prognosis of non-small cell lung cancer patients treated with immune checkpoint inhibitors. Transl Lung Cancer Res 10: 4511-4525, 2021.
43. Adams S, Schmid P, Rugo HS, Winer EP, Loirat D, Awada A, Cescon DW, Iwata H, Campone M, Nanda R, *et al*: Pembrolizumab monotherapy for previously treated metastatic triple-negative breast cancer: Cohort A of the phase II KEYNOTE-086 study. Ann Oncol 30: 397-404, 2019.
44. Hsu SK, Li CY, Lin IL, Syue WJ, Chen YF, Cheng KC, Teng YN, Lin YH, Yen CH and Chiu CC: Inflammation-related pyroptosis, a novel programmed cell death pathway, and its crosstalk with immune therapy in cancer treatment. Theranostics 11: 8813-8835, 2021.
45. Wu S, Pan R, Lu J, Wu X, Xie J, Tang H and Li X: Development and verification of a prognostic Ferroptosis-Related gene model in Triple-Negative breast cancer. Front Oncol 12: 896927, 2022.